Experimental and Analytical Investigations of the Flexural Behavior of Hollow ±55° Filament Wound GFRP Tubes

Dillon Betts[1*], Pedram Sadeghian[1], and Amir Fam[2]

ABSTRACT: The behavior of ±55° filament wound glass fiber-reinforced polymer (GFRP) tubes under flexural loading was examined experimentally and analytically. A total of 15 tubes were tested under four-point bending. The main test parameter was the ratio of inner diameter (D) to wall thickness (t), (D/t) ratio. The inner diameters of the tubes were 76 and 203 mm, while their wall thicknesses varied from 1.7 to 6.7 mm, giving D/t ratios of 20 to 75. All tests exhibited a nonlinear load-deflection response and a similar failure mechanism, namely a progressive tensile weakening until a sudden compression failure occurs. The tests showed that the moment capacity of the tubes increased with both tube diameter and nominal pressure rating. The tubes also exhibited a prolonged post-peak behavior. An iterative cross-sectional analytical technique was developed to model both the moment-curvature and load-deflection behavior of the tubes. The model accounts for the potential failure due to local buckling as well as compression failure and was shown to accurately predict the behavior of the tubes. A parametric study was performed to find the moment capacity of tubes with ratios beyond the range tested and was used to establish a simple design equation for moment capacity.

DOI: 10.1016/j.tws.2020.107246

KEYWORDS: GFRP tubes; angle-ply; flexure; experimental; analysis; nonlinear

---

[1] Department of Civil and Resource Engineering, Dalhousie University, 5268 DaCosta Row, Halifax, NS B3H 4R2, Canada.

[2] Department of Civil Engineering, Queen's University, Kingston, ON, K7L 3N6, Canada.

[*] dillonbetts@dal.ca (corresponding author)

1. INTRODUCTION

The use of fiber-reinforced polymers (FRPs) is constantly increasing for use in a variety of industries including aerospace, piping and, more recently, in sustainable infrastructure. These FRPs are popular due to their high specific strength and stiffness compared to traditional materials, their corrosion resistance and their design flexibility. FRPs can be manufactured into a variety of shapes including tubular structures, such as filament wound glass FRP (GFRP) tubes or sandwich pipes.

Many recent papers have mainly focused on the use of sandwich pipes or mortar FRP pipes which are able to resist high internal pressure loads [1,2], external pressure loads [3–5], transverse loads [6,7], and flexural loads [8,9]. The sandwich structure of the walls increases the wall stiffness which is particularly beneficial for applications such as buried pipelines [6] or deep-water pipelines [3,8]. Filament-wound GFRP tubes have become increasingly popular in the municipal and oil and gas sectors as a replacement for traditional metallic pipes. In this application, they are often subjected to internal pressure loads, resulting in a hoop stress to axial stress ratio of 2:1. For this reason, GFRP tubes have been studied extensively under internal pressure loading [1,10–16]. It has been noted in the literature [13,14] that thin-walled filament wound GFRP tubes with a ±55° winding angle with respect the axial direction of the tube are ideal for resisting this type of internal pressure loading. For this reason, ±55° GFRP tubes have become a readily available commercial product which makes them an economical choice for future applications in other industries. One such application that has been studied is the use of ±55° GFRP tubes filled with concrete, or concrete-filled-FRP tubes (CFFTs) [17–24], for use in structural applications such as columns or piles for buildings and bridges.

Using CFFTs as column structures provides several benefits. The GFRP tube provides confinement of the concrete thereby increasing the overall column strength. Additionally, because of their high corrosion resistance, FRP tubes act as a protective barrier for the column, especially important when the concrete is reinforced with steel. The FRP tubes also act as a stay-in-place formwork which increases the sustainability of structures by removing the need for temporary formwork thereby reducing construction waste. Shao and Mirmiran [25,26] examined the cyclic behavior of ±55° filament wound GFRP tubes filled with concrete. They tested the tubes under a four-point bending configuration under cyclic displacements ranging from ±6.4 mm to ±127 mm and found that the ±55° CFFTs exhibited a ductile, elastoplastic behavior. Zhu et al. [27] modelled the ±55° tubes tested by Shao and Mirmiran [25] using the finite element method (FEM). The results of their study showed that ±55° CFFTs can be modelled using commercially available software. Using their FEM model, they performed a parametric study which showed that the strength and ductility of ±55° CFFTs decreased when the FRP thickness was decreased and when the diameter to thickness (D/t) ratio was increased. Zhu et al. [28] performed experiments on ±55° CFFTs under cyclic loading applied at the top connect of CFFT column structures. These tests showed that CFFTs were stronger and more ductile than similar traditional reinforced concrete (RC) columns. Echevvaria et al. [29] tested RC columns and ±55° CFFTs under blast loading. Their tests showed that the post-blast CFFTs exhibited less loss in strength and ductility than their RC counterparts. Gemi et al. [30] tested ±55° CFFTs and plain concrete specimens under axial compression using both Portland cement and expansive cement. The results of the tests showed that the CFFT specimens were stronger and more ductile. However, in order to develop design equations for these types of structures, there is a need to have a deeper understanding of the behavior of the individual components, especially the filament-wound GFRP tubes.

To overcome this gap in the literature, recent studies have focused on ±55° tubes and have investigated their behavior under pure axial tensile loads [14,31,32], pure axial compression loads [32] as well as their flexural strength using maximum stress criterion [33]. Studies have been performed on the flexural behavior of carbon FRP (CFRP) tubes [34,35] and various FRP tubes for specific applications, such as spoolable pipes [36–40] and transmission line poles [41]. However, research on the flexural behavior of hollow ±55° GFRP tubes under remains limited, especially in considering the nonlinear behavior observed in previous studies [32]. In this study, the behavior of ± 55° GFRP tubes under flexural loads is thoroughly investigated experimentally by testing hollow tubes with different diameters and wall thicknesses. An analytical model based on a cross sectional analysis is developed to predict their load-deflection behavior and ultimate bending strength. The model captures the nonlinear flexural behavior of these tubes by considering the nonlinear behavior of the material in tension and compression.

2. EXPERIMENTAL PROGRAM

As a part of this study, 15 filament-wound GFRP tubes were tested under four-point bending. Tubes with diameters of 76 mm or 203 mm were supplied by a local manufacturer (RPS Composites, Mahone Bay, NS, Canada). All tubes were manufactured using Electrical/Chemical Resistant (ECR) glass fibers and a vinylester resin (Ashland Derakane 411) and had a fiber volume fraction of 50.2% and a fiber angle of ±55° with an error of ±2°. For the 203 mm diameter tubes, three different wall thicknesses were supplied and for the 76 mm diameter tubes, two different wall thicknesses were supplied. The test matrix and test set-up will be presented in this section.

2.1. Test Matrix

The main test parameter was the D/t ratio. Tubes with two inner diameters (76 mm or 203 mm) and three nominal internal pressure ratings as reported by the manufacturer (350 kPa, 700 kPa or 1050 kPa) were tested. The nominal internal pressure ratings are related to both the tube diameter and wall thickness. The wall thickness increased from 1.7 mm to 6.7 mm with nominal pressure rating. To distinguish specimens, the following naming convention was used: PX-DY, where X is the nominal pressure rating in kPa, and Y is the inner diameter rounded to the nearest mm. For example, a group of tubes with pressure ratings of 350 kPa and inner diameters of 76 mm would be identified as P350-D76. The test matrix, including inner diameter, span length, and fiber architecture is presented in Table 1.

2.2. Test Setup and Instrumentation

The tubes were supplied in 7620 mm lengths by a manufacturer and were cut to the required length using a band saw. The 203 mm diameter tubes were cut to a length of 3250 mm and were tested at a span length of 3048 mm with a constant moment zone of 457 mm. The 76 mm diameter tubes were cut to a length of 1245 mm and were tested at a span length of 1143 mm with a constant moment zone of 171 mm.

The test set-up in presented in Figure 1. Longitudinal electric resistance strain gauges were applied to opposing sides (i.e. top and bottom, separated by 180°) at midspan. On the bottom side a string potentiometer connection point was adhered to the midspan using an epoxy-based glue. On the 203 mm diameter tubes, a small plate was attached to each side at midspan such that an LVDT could be placed to measure the change in diameter (ovalization). As shown in Figure 1, custom steel support fixtures were fabricated for testing the 76 mm and 203 mm diameter tubes. To avoid localised damaged at the supports and loading points, neoprene pads were placed between the steel supports and the specimen. A steel roller was used at each support and loading point. Each test was performed at approximately 15 mm/min and data was sampled at 10 Hz.

3. EXPERIMENTAL RESULTS AND DISCUSSIONS

Based on the recorded load, deflection and strain data, the load-deflection behavior was determined and analysed. The data processing was completed using a Python program written using the scientific package, Anaconda. The results of the tests are presented in Table 2 and will be discussed in this section.

3.1. Failure Modes

A photo of the typical failure exhibited by all specimens is presented in Figure 2. The typical failure began with audible cracking which was observed before any visible indication of failure. Based on test observations, the audible cracking originated at the bottom surface of the tubes where there was a state of tensile stress due to the flexural loading. Previous studies have focused on the tensile behavior [14,31,32] and the biaxial behavior (including approximate tensile behavior) [42–44] of filament wound GFRP tubes. Based on the observations from the study by Bai et al [14], the first phase of failure observed through audible cracking is due to matrix cracking in resin rich areas, such as the outer gel coat. The second phase of failure observed in this study was the formation of progressive transverse matrix cracks observed at the bottom surface at midspan. These matrix cracks were also observed in the previous studies [14,31,42–44]. The tensile cracks grew and propagated towards the top until, at a critical point, a sudden ultimate failure occurred in compression at the top face. Note that while the failures shown in Figure 2 exhibit angled failure planes, this is due to the state of tension in the bottom side of the tube and not due to shear. This is verified by the fact that all failures began within the constant moment zone. Note that, as shown in Figure 3, specimens P1050-D203-1 and P1050-D203-3 did not experience ultimate failure as the maximum stroke of the actuator was reached. However, based on test observations and a comparison with specimen P1050-D203-2, it is assumed that these specimens were close to ultimate failure at the end of the test and that they would exhibit the same failure mode as all other specimens.

3.2. Load-Deflection Behavior

The load-deflection behavior of the tubes is presented in Figure 3 and the ultimate conditions are presented in Table 2. For each case, three identical tubes were tested. As discussed earlier, during the tests, audible cracking was noted before any visible indication of failure. The load at which audible cracking occurred was recorded and shown in Figure 3. Note that for the 76 mm diameter tubes, the audible cracking began at approximately 25 mm of deflection for both specimen types, while it began at approximately 50 mm for all 203 mm diameter tubes.

The maximum load increased with wall thickness for both the 76 mm and 203 mm diameter tubes. For the 76 mm diameter tubes, the P1050 tubes (i.e. thicker walls) resisted an average peak load of 8.5 kN, an increase of 132% from the P350 tubes which resisted a peak load of 3.6 kN. For the 203 mm tubes the P1050 specimens resisted an average peak load of 31.2 kN which is an increase of 53% from the P700 specimens (20.5 kN) and 205% from P350 specimens (10.2 kN).

While there was a significant difference in the flexural load capacity of the tested 76 mm diameter tubes, the ultimate deflection was not significantly affected by wall thickness. The P350-D76 tubes had an ultimate deflection of 66 mm whereas the P1050-D76 tubes had an ultimate deflection of 64 mm. The same pattern is observed for the P350 and P700 203 mm diameter tubes showing an average ultimate deflection of 93 mm and 86 mm, respectively. However, the P1050-D203 tubes showed a significantly higher ultimate deflection of 118 ± 1 mm, a 37% increase from the P700-D203 tubes. This suggests that the ultimate compression failure of P1050-D203 tubes may have been initialized by a different failure mechanism than the others, that is material failure rather than stability failure. It is difficult to verify this hypothesis based on the test observations as ultimate failure occurred suddenly. However, Figure 3 shows that after the start of audible cracking, the lead-deflection diagrams of the P350-D203 (Figure 3c) and P700-D203 (Figure 3d) tubes lose steadiness whereas the

P1050-D203 load-deflection diagram (Figure 3e) is stable until failure. Therefore, it is concluded that the ultimate compression side failure of the P1050-D203 tubes was initialized by material failure whereas the P350 and P700 compression failures were initialized by stability. Additionally, based on the stable load-deflection diagrams of the P350-D76 (Figure 3a) and P1050-D76 tubes (Figure 3b), it is also likely that the ultimate compression side failure in these tubes was initialized by material failure.

For all tests, the tubes exhibited a nonlinear loading path. This is due to the intrinsic nonlinear stress-strain behavior of the tubes in tension and compression. In a previous study, Betts et al. [32] tested the same GFRP tubes under uniaxial tension and compression. They showed that ±55° GFRP tubes exhibit a nonlinear response in both tension and compression due to the influence of the nonlinear shear behavior in the principal loading direction. Additionally, as shown in Figure 3, all specimens retained significant load capacity after the peak load. This post-peak behavior is due to the progressive failure of the tension side of the tubes observed during the flexural tests. This corresponds with the post-peak behavior of tubes loaded under uniaxial tension observed by Betts et al. [32]. As the stress in tension slowly decreases, the flexural load capacity decreases. This effect is discussed at length in the analysis section.

3.3. Ovalization

For the 203 mm diameter tubes, ovalization was measured and is presented in Figure 4. Note that due to the progressive tensile failure, the plates used to measure ovalization separated from the specimens and therefore ovalization measurements were not available to specimen failure for some specimens. Additionally, based on the data, specimen P350-D203-3 was labelled as an outlier as it exhibited significantly more ovalization than specimens P350-D203-1 and P350-D203-2. This outlier was likely caused by an error with the test set-up or data acquisition and therefore it was not presented.

Looking at Figure 4, the P1050 specimens are stiffer in terms of exhibiting lower ovalization than the other two specimen types. The P350 and P700 specimens exhibited similar ovalization behavior. The maximum recorded ovalization for each specimen is presented in Table 3.

4. ANALYTICAL STUDY

This section introduces the development of an analytical model to predict the behavior of ± 55° GFRP tubes under flexural loading. Because flexural loading induces a state of compression in the top section of the tube and a state of tension in the bottom section of the tube, the model was based on a cross-sectional analysis using the known stress-strain behavior of these tubes in both compression and tension. The model predicts the failure of the tubes based on the stability failure of thin shells.

4.1. Constitutive Relationships

The mechanical behavior of ±55° GFRP tubes has been shown to be nonlinear in both tension and compression in a previous study [32]. In tension, these tubes have exhibited an approximately parabolic pre-peak behavior followed by an approximately linear post-peak behavior and were modelled as such. The parabolic pre-peak model was based on Eq. 1.

$$\sigma_t = A_1\epsilon_t^2 + B_1\epsilon_t + C_1 \tag{1}$$

where σ_t is the tensile stress in MPa, ε_t is tensile strain in mm/mm, and A_t, B_t and C_t are constants which were determined using the following boundary conditions (BC): BC1: $\{\varepsilon_t = \varepsilon_{tu}; \sigma_t = \sigma_{tu}\}$; BC2: $\{\varepsilon_t = 0; \sigma_t = 0\}$ and; BC3: $\{\varepsilon_t = 0; d\sigma_t/d\varepsilon_t = E_t\}$, where σ_{tu} is the ultimate tensile strength, ε_{tu} is the tensile strain corresponding to the ultimate stress and E_t is the tensile modulus of elasticity. The post-peak tensile behavior was modelled as linear softening using BC1 and the following additional boundary condition: BC4: $\{\varepsilon_t = 6\varepsilon_{tu}; \sigma_t = 0.6\sigma_{tu}\}$. This additional boundary condition was proposed by Betts et al [32] as a way to model the post-peak tensile behavior of these tubes based on the results of their uniaxial tension tests. As their tensile tests did not experience ultimate failure, they assumed failure at a 40% decrease from the peak tensile stress. Based on their test observations, the corresponding failure strain was six times the strain corresponding to the peak stress. By including this post-peak tensile material model in the analysis, the progressive tensile failure behavior of the tubes was incorporated into the analysis empirically.

By solving for the constants, the tensile stress-strain relation of the GFRP tubes becomes:

$$\sigma = \begin{cases} (\sigma_u - E\epsilon_u)\dfrac{\epsilon^2}{\epsilon_u^2} + E\epsilon, & \epsilon \le \epsilon_u \\ -\left(\dfrac{0.4\sigma_u}{5}\right)\dfrac{\epsilon}{\epsilon_u} + \dfrac{5.4\sigma_u}{5}, & \epsilon_u < \epsilon \le 6\epsilon_u \end{cases} \tag{2}$$

In compression, the tubes have exhibited an approximately cubic relationship until failure which can be described by Eq. 3.

$$\sigma_c = A_c\epsilon_c^3 + B_c\epsilon_c^2 + C_c\epsilon_c + D_c \tag{3}$$

where σ_c is the compressive stress in MPa. The constants can be determined by using the following boundary conditions: BC5: $\{\varepsilon_c = \varepsilon_{cu};\ \sigma_c = \sigma_{cu}\}$; BC6: $\{\varepsilon_c = 0;\ \sigma_c = 0\}$; BC7: $\{\varepsilon_c = 0;\ d\sigma_c/d\varepsilon_c = E_c\}$ and; BC8: $\{\varepsilon_c = \varepsilon_{cu};\ d\sigma_c/d\varepsilon_c = 0\}$, where σ_{cu} is the ultimate compressive stress, ε_{cu} is the compressive strain corresponding to the ultimate compressive stress and E_c is the compressive modulus of elasticity. By solving for the constants, the equation relating compressive stress and strain is given in Eq. 4.

$$\sigma_c = (E\epsilon_{cu} - 2\sigma_{cu})\frac{\epsilon_c^3}{\epsilon_{cu}^3} + (3\sigma_{cu} - 2E_c\epsilon_{cu})\frac{\epsilon_c^2}{\epsilon_{cu}^2} + E_c\epsilon_c \tag{4}$$

The models were both verified against test data from a previous study [32]. The verification of the tension and compression models are shown in Figures 5a and 5b, respectively.

4.2. Model Description

The model presented in this section was developed to predict the moment-curvature and load-deflection behavior of the ±55° GFRP tubes using the known nonlinear material behavior of the tubes in tension and compression. In order to incorporate the material behavior an in-depth cross-sectional analysis approach was used. The cross-sectional analysis diagram is shown in Figure 6 and the procedure is shown in Figure 7. The effect of ovalization on the moment of inertia of the tubes is shown in Table 3. It was determined that, within the range of D/t ratios investigated in this study, ovalization had little effect on the moment of inertia of the tubes. Additionally, in many civil engineering applications the tube may be braced by external backfill soil as in pipelines or internal concrete fill as with CFFTs, so ovalization will likely be insignificant. As such, ovalization was not included in the model. Note that the wall thicknesses remain constant throughout the modeling to be consistent with the material properties which are based on the uniaxial tension and compression tests which do not consider geometrical changes.

To determine the moment-curvature behavior, it is first necessary to determine the neutral axis depth, c, by equating the force in tension, F_t and the force in compression, F_c. Based on Figure 6, the equation for F_c is presented in Eq. 5. The force in tension for any strain profile can be determined similarly based on the appropriate case from Figure 6. As the model is based on the nonlinear material behavior of the tubes, the neutral axis changes based on the state of stress in the tube and must be calculated at each model step.

$$F_c = \int_{r_o-c}^{r_i} 2\sigma_c \left(\sqrt{r_o^2 - y^2} - \sqrt{r_i^2 - y^2}\right) dy + \int_{ri}^{r_o} 2\sigma_c \sqrt{r_o^2 - y^2} dy \qquad (5)$$

where r_i is the inner tube radius, r_o is the outer tube radius, c is the distance from the neutral axis to the extreme compression fiber, σ_c is the formula for tube compressive stress written in terms of c and

y is the distance from the mid-plane. The tension force is determined similarly based on the case shown in Figure 6.

The only unknown is the neutral axis depth, c. As shown in Figure 7, this is found by first assuming that $c = r_o$ and then iterating the procedure until F_t / F_c becomes 1.0 ± 0.001. Once the neutral axis depth is determined, the moment area of the force in compression, Q_c, and tension, Q_t, can be found. The equation for Q_c is presented as Eq. 6. Again, Q_t is not shown, but can be determined similarly based on the appropriate case in Figure 6.

$$Q_c = \int_{r_o - c}^{r_i} 2\sigma_c(y - r_o + c)\left(\sqrt{r_o^2 - y^2} - \sqrt{r_i^2 - y^2}\right)dy + \int_{ri}^{r_o} 2\sigma_c(y - r_o + c)\sqrt{r_o^2 - y^2}dy \tag{6}$$

The moment and curvature can then be determined at each point using Eq. 7 and Eq. 8, respectively.

$$M_i = Q_c + Q_t \tag{7}$$

$$\psi_i = \frac{\epsilon_c}{c} \tag{8}$$

where M_i is the moment and ψ_i is the curvature. Based on the moment-curvature behavior, the load-deflection behavior can be determined based on Figure 8 and using Eq. 9 and Eq. 10.

$$P_i = \frac{2M_i}{a} \tag{9}$$

$$\Delta_i = \int_0^a x\psi dx + \frac{\psi_i a}{2}\left(a + \frac{b}{4}\right) \tag{10}$$

where P_i is the load, Δ_i is the deflection at midspan, a is the distance from the support to the nearest load point and b is the distance between load points.

Thus far, the model has been developed based on material failure. However, as observed by Betts et al. [32], these tubes can be susceptible to stability failure. Therefore, it is necessary to consider the potential premature failure due to wall buckling. Stability failure can be predicted for linear elastic isotropic materials using the equation for critical stress developed by Timoshenko and Gere [45], presented below:

$$\sigma_{cr} = \frac{Et}{r\sqrt{3(1-v^2)}} \tag{11}$$

where σ_{cr} is the critical compressive stress where buckling would occur, E is the modulus of elasticity of the isotropic material, t is the cylinder wall thickness, r is the radius to the middle of the wall and v is the Poisson's ratio.

As the tubes in question are fabricated using ±55° GFRPs, they can be considered as an orthotropic material. Therefore, it is necessary to consider their behavior in the axial and circumferential directions. To estimate when local buckling would occur, a buckling envelope was established by determining the lower critical buckling stress, σ_{crl}, based on the modulus of elasticity and Poisson's ratio in the axial direction and the upper critical buckling stress, σ_{cru}, based on the modulus of elasticity and Poisson's ratio in the hoop direction. The moduli were calculated using the Classical Lamination Theory (CLT) based on the properties of a 0° unidirectional glass-epoxy laminate from the typical properties provided by Daniel and Ishai [46]. The axial modulus, axial Poisson's ratio, hoop modulus and hoop Poisson's ratio were calculated using CLT and were found to be 10.6 GPa, 0.303, 14.3 GPa and 0.409 respectively.

Additionally, it is known that the stress-strain relationship of the GFRP tubes is nonlinear [32] and therefore they cannot be considered as a linear-elastic material. Timoshenko and Gere [45] proposed that in this situation, the modulus of elasticity, E, in the Eq. 11, be replaced by the tangent modulus, E_{tan}. In future studies, the prediction of the critical compressive buckling stress should be improved by considering the orthotropic nature of the tubes directly.

4.3. Verification

The model verification of the load-deflection and moment-curvature plots are presented in Figure 9 and Figure 10, respectively. The figures show that the lower critical buckling stress, σ_{crl}, predicts the failure load well. This is likely because the modulus in the axial direction is lower than the modulus in the hoop direction and therefore controls the mode of failure. The lower critical buckling stress has been considered the failure condition for the model. A comparison of the test and model results are presented in Table 2, which shows that the test/model ratio for the peak moment is 1.03. Figures 10 and 11 show that the model can accurately predict the behavior of the tubes. They also show that the model would overpredict the behavior of the tubes if the premature stability failure was not accounted for.

4.4. Parametric Study

Using the model developed in this study, a parametric study was performed to examine the effect of diameter to thickness ratio (D/t) and the span length to diameter ratio (L/D). In this section the effects of both D/t and L/D are examined and discussed. Additionally, a relationship between tube moment capacity and the D/t ratio is presented. The test matrix for the parametric study is presented in Table 4.

4.4.1. Effect of Diameter to Thickness Ratio

To examine the effect of the D/t ratio on the tube behavior, tubes with the same diameters as those tested, namely 76.2 mm and 203.2 mm, were modelled with various thicknesses. Additionally, tubes with larger diameters of 304.8 mm and 406.4 mm and various D/t ratios were also modelled. In total, 35 cases with varying pipe diameters and D/t ratios were examined. In each model, the L/D ratio was set as 15. Note that, as discussed previously, the models were assumed to fail at the lower critical buckling stress, σ_{crl}.

Figure 11 shows the effect of the D/t ratio on both the load-deflection and moment-curvature behavior of the tubes. Both ultimate load-capacity, stiffness, flexural rigidity and ultimate deflection decrease with an increase in D/t. As the D/t decreases, the post-peak behavior is also prolonged. This is due to the progressive tensile failure mechanism. As the tensile failure of the bottom surface progresses, the compression zone gets smaller, increasing the compression stress in the top of the tube. This causes stability failure to occur earlier in the thinner tubes (ie. higher D/t), which does not allow for the tubes to experience a post-peak behavior. This is consistent with the test results presented in Figure 3; however, it is more apparent in Figure 11 as more D/t ratios were investigated.

The effect of D/t ratio on tube moment capacity is presented in Figure 12. To directly compare all tube diameters, the moment was normalized based on the inner diameter and plotted against the D/t ratio. Based on the model data, a power relationship with an R^2 value of 0.995 was found and is presented in Eq. 12.

$$\frac{M_u}{D^3} = 180.2\left(\frac{D}{t}\right)^{-1.23} \tag{12}$$

where M_u is the peak moment of the tube, D is the tube inner diameter and t is the tube wall thickness. The test data was plotted to verify the relationship predicted by the model results. The normalized average peak moment of each test specimen type is also shown in Figure 12 and follows the same trend exhibited by the models. Equation 12 is a simple design tool that can be used for typical ±55° GFRP tubes subjected to flexure.

4.4.2. Effect of the Span Length to Diameter Ratio

To examine the effect of the L/D ratio on tube flexural behavior, the models of the tubes tested (L/D = 15) were compared with models of the same tubes with L/D ratios of 10 and 20. The effect of L/D on the load-deflection behavior of the tubes is presented in Figure 13. As the model does not consider shear deflection, the moment-curvature behavior was not affected by L/D and therefore not presented.

As would be expected, the ultimate load capacity and stiffness increase with a decrease in span length, whereas the ultimate deflection decreases. While the length of the post-peak zone decreases with a decrease in L/D, this is due to the change in the overall stiffness and it can be said that the L/D ratio has no significant effect on the post-peak behavior of the tubes. This can be verified by looking at Figure 13 and the P1050-D76 tube. For each L/D, tube failure occurs at 82% of the ultimate load capacity. Because shear is not considered in the model, this is expected. The material behavior does not change due to a change in L/D and therefore, the post-peak behavior is unaffected.

Future studies in this area should further verify the model and parametric study with more tests of ±55° tubes with different diameters, D/t ratios and L/D ratios. Additionally, more tubes should be tested and analysed under combined axial and flexural loads.

5. CONCLUSIONS

As a part of this study, fifteen ±55° filament wound GFRP tubes were tested under four-point bending. The flexural behavior of ±55° tubes presented in this study is beneficial to the field as these tubes have seen increased use in infrastructure applications such as concrete-filled FRP tubes (CFFTs). The main parameters of the tests were the effects of tube diameter (76 mm and 203 mm) and nominal tube pressure capacity (350 kPa, 700 kPa and 1050 kPa), which is related to the wall thickness, on flexural capacity. Based on the results of the tests, the following observations were made:

- The ±55° GFRP tubes all failed in a similar ductile manner: a progressive post-peak tensile softening until a sudden compression failure occurs due to local buckling or material failure in compression.
- The GFRP tubes exhibited a nonlinear moment-curvature and load-deflection response and a prolonged post-peak behavior. The post-peak behavior was attributed to the progressive

tensile failure of the tubes evidenced by audible cracking and visible damage observed during in the current study and in uniaxial tension tests from previous studies.

- The tubes showed an increase in flexural capacity with a decrease in D/t ratio when compared to other tubes with the same inner diameter. For the 76 mm diameter tubes, when D/t ratio was decreased from 45 to 20, the tube capacity increased by 132%. For the 203 mm diameter tubes, when the D/t ratio decreased from 75 to 30, the flexural capacity increased by 205%.

A novel analytical model was developed based on a cross-sectional analysis of the tubes. The model effectively incorporated the nonlinear material behavior of the tubes in both tension and compression, including the post-peak tensile behavior of the tubes. Using the developed model, a parametric study was performed to show the behavior of tubes with thicker walls and larger diameters. Based on the analytical study, the following conclusions were drawn:

- The analytical model, accounting for material nonlinearity in tension and compression, was shown to accurately predict the tube moment capacity and the full behavior until stability failure occurs by local buckling.
- Based on a parametric study using the developed model, a design equation was presented which relates the normalized moment capacity and the D/t ratio for ±55° tubes. This relationship was successfully verified using the test data.

6. DATA AVAILABILITY

The raw/processed data required to reproduce these findings cannot be shared at this time due to technical or time limitations.

7. ACKNOWLEDGEMENTS

The authors would like to thank Jesse Keane, Brian Kennedy and Jordan Maerz for their assistance in the lab. The authors would also like to acknowledge and thank the Natural Sciences and Engineering Research Council of Canada (NSERC), Queen’s University, and Dalhousie University for their financial support and RPS Composites (Mahone Bay, NS, Canada) for in-kind contribution.

8. REFERENCES

[1] Rafiee R, Reshadi F. Simulation of functional failure in GRP mortar pipes. Compos Struct 2014;113:155–63. doi:10.1016/j.compstruct.2014.03.024.

[2] Rafiee R, Mazhari B. Evaluating long-term performance of Glass Fiber Reinforced Plastic pipes subjected to internal pressure. Constr Build Mater 2016;122:694–701. doi:10.1016/j.conbuildmat.2016.06.103.

[3] Arjomandi K, Taheri F. Stability and post-buckling response of sandwich pipes under hydrostatic external pressure. Int J Press Vessel Pip 2011;88:138–48. doi:10.1016/j.ijpvp.2011.02.002.

[4] Arjomandi K, Taheri F. A new look at the external pressure capacity of sandwich pipes. Mar Struct 2011;24:23–42. doi:10.1016/j.marstruc.2010.12.001.

[5] Arjomandi K, Taheri F. Elastic buckling capacity of bonded and unbonded sandwich pipes under external hydrostatic pressure. J Mech Mater Struct 2010;5:391–408. doi:10.2140/jomms.2010.5.391.

[6] Rafiee R, Habibagahi MR. On The Stiffness Prediction of GFRP Pipes Subjected to Transverse Loading. KSCE J Civ Eng 2018;22:4564–72. doi:10.1007/s12205-018-2003-5.

[7] Rafiee R, Habibagahi MR. Evaluating mechanical performance of GFRP pipes subjected to transverse loading. Thin-Walled Struct 2018;131:347–59. doi:10.1016/j.tws.2018.06.037.

[8] Arjomandi K, Taheri F. Bending capacity of sandwich pipes. Ocean Eng 2012;48:17–31.

doi:10.1016/j.oceaneng.2011.09.014.

[9] Xia M, Takayanagi H, Kemmochi K. Bending behavior of filament-wound fiber-reinforced sandwich pipes. Compos Struct 2002;56:201–10. doi:10.1016/S0263-8223(01)00181-7.

[10] Rafiee R. On the mechanical performance of glass-fibre-reinforced thermosetting-resin pipes: A review. Compos Struct 2016;143:151–64. doi:10.1016/j.compstruct.2016.02.037.

[11] Rafiee R, Amini A. Modeling and experimental evaluation of functional failure pressures in glass fiber reinforced polyester pipes. Comput Mater Sci 2015;96:579–88. doi:10.1016/j.commatsci.2014.03.036.

[12] Rafiee R, Mazhari B. Simulation of the long-term hydrostatic tests on Glass Fiber Reinforced Plastic pipes. Compos Struct 2016;136:56–63. doi:10.1016/j.compstruct.2015.09.058.

[13] Xing J, Geng P, Yang T. Stress and deformation of multiple winding angle hybrid filament-wound thick cylinder under axial loading and internal and external pressure. Compos Struct 2015;131:868–77. doi:10.1016/j.compstruct.2015.05.036.

[14] Bai J, Seeleuthner P, Bompard P. Mechanical behaviour of ±55° filament-wound glass-fibre/epoxy-resin tubes: I. Microstructural analyses, mechanical behaviour and damage mechanisms of composite tubes under pure tensile loading, pure internal pressure, and combined loading. Compos Sci Technol 1997;57:141–53. doi:10.1016/S0266-3538(96)00124-8.

[15] Xia M, Takayanagi H, Kemmochi K. Analysis of multi-layered filament-wound composite pipes under internal pressure. Compos Struct 2001;53:483–91. doi:10.1016/S0263-8223(01)00061-7.

[16] Rafiee R. Apparent hoop tensile strength prediction of glass fiber-reinforced polyester pipes. J Compos Mater 2013;47:1377–86. doi:10.1177/0021998312447209.

[17] Teng JG, Chen JF, Smith ST, Lam L. Behaviour and strength of FRP-strengthened RC structures: a state-of-the-art review. Proc Inst Civ Eng - Struct Build 2003;156:51–62. doi:10.1680/stbu.2003.156.1.51.

[18] Lam L, Teng JG. Ultimate Condition of Fiber Reinforced Polymer-Confined Concrete. J Compos Constr 2004;8:539–48. doi:10.1061/(ASCE)1090-0268(2004)8:6(539).

[19] Bakis CE, Bank LC, Brown VL, Cosenza E, Davalos JF, Lesko JJ, et al. Fiber-Reinforced Polymer Composites for Construction - State-of-the-Art Review. J Compos Constr 2002. doi:10.1061/(ASCE)1090-0268(2002)6:2(73).

[20] Mandal S, Hoskin A, Fam A. Influence of Concrete Strength on Confinement Effectiveness of Fiber-Reinforced Polymer Circular Jackets 2005:383–93.

[21] Berthet JF, Ferrier E, Hamelin P. Compressive behavior of concrete externally confined by composite jackets: Part A: experimental study. Constr Build Mater 2005;19:223–32. doi:10.1016/j.conbuildmat.2005.01.029.

[22] Sadeghian P, Fillmore B. Strain distribution of basalt FRP-wrapped concrete cylinders. Case Stud Constr Mater 2018;9:e00171. doi:10.1016/j.cscm.2018.e00171.

[23] Fam A, Flisak B, Rizkalla S. Experimental and Analytical Investigations of Concrete-Filled Fiber-Reinforced Polymer Tubes Subjected to Combined Bending and Axial Loads. ACI Struct J 2003;100:499–509.

[24] Fam AZ, Rizkalla SH. Behavior of Axially Loaded Concrete-Filled Circular FRP Tubes. ACI Struct J 2001;98:280–9.

[25] Shao Y, Mirmiran A. Nonlinear cyclic response of laminated glass FRP tubes filled with concrete. Compos Struct 2004;65:91–101. doi:10.1016/j.compstruct.2003.10.009.

[26] Shao Y, Mirmiran A. Experimental Investigation of Cyclic Behavior of Concrete-Filled

Fiber Reinforced Polymer Tubes. J Compos Constr 2005;9:263–73. doi:10.1061/(asce)1090-0268(2005)9:3(263).

[27] Zhu Z, Ahmad I, Mirmiran A. Fiber element modeling for seismic performance of bridge columns made of concrete-filled FRP tubes. Eng Struct 2006;28:2023–35. doi:10.1016/j.engstruct.2006.03.031.

[28] Zhu Z, Ahmad I, Mirmiran A. Seismic Performance of Concrete-Filled FRP Tube Columns for Bridge Substructure. J Bridg Eng 2006;11:359–70. doi:10.1061/(asce)1084-0702(2006)11:3(359).

[29] Echevarria A, Zaghi AE, Chiarito V, Christenson R, Woodson S. Experimental Comparison of the Performance and Residual Capacity of CFFT and RC Bridge Columns Subjected to Blasts. J Bridg Eng 2015;21:04015026. doi:10.1061/(asce)be.1943-5592.0000762.

[30] Gemi L, Köroğlu MA, Ashour A. Experimental study on compressive behavior and failure analysis of composite concrete confined by glass/epoxy ±55° filament wound pipes. Compos Struct 2018;187:157–68. doi:10.1016/j.compstruct.2017.12.049.

[31] Khalifa A Ben, Zidi M, Abdelwahed L. Mechanical characterization of glass/vinylester ±55° filament wound pipes by acoustic emission under axial monotonic loading. Comptes Rendus - Mec 2012;340:453–60. doi:10.1016/j.crme.2012.02.006.

[32] Betts D, Fam A, Sadeghian P. Investigation of the Stress-Strain Constitutive Behavior of ±55° Filament Wound GFRP Pipes in Compression and Tension. Compos Part B 2019:243–52.

[33] Natsuki T, Takayanagi H, Tsuda H, Kemmochi K. Prediction of bending strength for filament-wound composite pipes. J Reinf Plast Compos 2003;22:695–710. doi:10.1177/0731684403022008002.

[34] Huang Z, Qian X, Su Z, Pham DC, Sridhar N. Experimental investigation and damage simulation of large-scaled filament wound composite pipes. Compos Part B Eng 2020;184:107639. doi:10.1016/j.compositesb.2019.107639.

[35] Akkus N, Kawahara M. Bending behaviors of thin composite pipes with reinforcing nodes. Mater Sci Res Int 2000;6:131–5. doi:10.2472/jsms.49.6appendix_131.

[36] Ashraf MA, Morozov E V., Shankar K. Flexure analysis of spoolable reinforced thermoplastic pipes for offshore oil and gas applications. J Reinf Plast Compos 2014;33:533–42. doi:10.1177/0731684413491442.

[37] Yu K, Morozov E V., Ashraf MA, Shankar K. Analysis of flexural behaviour of reinforced thermoplastic pipes considering material nonlinearity. Compos Struct 2014;119:385–93. doi:10.1016/j.compstruct.2014.09.015.

[38] Menshykova M, Guz IA. Stress analysis of layered thick-walled composite pipes subjected to bending loading. Int J Mech Sci 2014;88:289–99. doi:10.1016/j.ijmecsci.2014.05.012.

[39] Yu K, Morozov E V., Ashraf MA, Shankar K. Numerical analysis of the mechanical behaviour of reinforced thermoplastic pipes under combined external pressure and bending. Compos Struct 2015;131:453–61. doi:10.1016/j.compstruct.2015.05.033.

[40] Bai Y, Tang J, Xu W, Cao Y, Wang R. Collapse of reinforced thermoplastic pipe (RTP) under combined external pressure and bending moment. Ocean Eng 2015;94:10–8. doi:10.1016/j.oceaneng.2014.10.002.

[41] Mitchell J, Fam A. Tests and Analysis of Cantilevered GFRP Tubular Poles with Partial Concrete Filling. J Compos Constr 2010;14:115–24. doi:10.1061/(asce)cc.1943-5614.0000041.

[42] Carroll M, Ellyin F, Kujawski D, Chiu AS. The rate-dependent behaviour of ± 55 ° filament-

wound glass-fibre/epoxy tubes under biaxial loading. Compos Sci Technol 1995;55:391–403. doi:10.1016/0266-3538(95)00119-0.

[43] Ellyin F, Carroll M, Kujawski D, Chiu AS. The behavior of multidirectional filament wound fibreglass/epoxy tubulars under biaxial loading. Compos Part A Appl Sci Manuf 1997;28:781–90. doi:10.1016/S1359-835X(97)00021-3.

[44] Mertiny P, Ellyin F, Hothan A. An experimental investigation on the effect of multi-angle filament winding on the strength of tubular composite structures. Compos Sci Technol 2004;64:1–9. doi:10.1016/S0266-3538(03)00198-2.

[45] Timoshenko S, Gere J. Theory of Elastic Stability. Second Ed. McGraw-Hill; 1963.

[46] Daniel IM, Ishai O. Engineering mechanics of composite materials. Mech Compos Mater 1994. doi:10.1016/B978-0-08-006421-5.50049-6.

Table 1. Test Matrix

Specimen Group	Nominal Pressure Rating (kPa)	No. of Identical Specimens	Inner Diameter (mm)	Span (mm)	Constant Moment Zone (mm)	Cross Sectional Area (mm^2)	Wall Thickness (mm)	Diameter-Thickness Ratio (D/t)	Fiber Architecture * (°)
P350-D76	350	3	76.2	1143	171	416.5	1.7	45	$[\pm 55]_2$
P1050-D76	1050	3	76.2	1143	171	964.4	3.8	20	$[\pm 55]_5/+55$
P350-D203	350	3	203.2	3048	457	1741.5	2.7	75	$[\pm 55]_2/+55$
P700-D203	700	3	203.2	3048	457	3103.0	4.7	43	$[\pm 55]_4$
P1050-D203	1050	3	203.2	3048	457	4404.6	6.7	30	$[\pm 55]_5$

** fiber architecture degrees with respect to the longitudinal axis of the tubes*

Table 2. Test and Analysis Results

Specimen Group	Peak Load (kN)			Deflection at Peak Load (mm)			Peak Moment (kN-m)		
	Test *	Model †	Test/Model	Test	Model	Test/Model	Test	Model	Test/Model
P350-D76	3.64 ± 0.12	2.76	1.32	66 ± 11	35	1.90	0.86 ± 0.02	0.67	1.28
P1050-D76	8.46 ± 0.30	7.97	1.06	64 ± 6	53	1.20	2.00 ± 0.03	1.94	1.03
P350-D203	10.25 ± 0.27	9.87	1.04	93 ± 20	76	1.23	6.64 ± 0.18	6.40	1.04
P700-D203	20.47 ± 0.46	23.00	0.89	86 ± 6	112	0.77	13.26 ± 0.30	14.90	0.89
P1050-D203 ‡	31.25 ± 1.01	34.97	0.89	118 ± 1	130	0.90	20.24 ± 0.66	22.65	0.89
Average			1.04 ± 0.18			1.20 ± 0.44			1.03 ± 0.16

** Test results are the average of three tests*

† Model failure is considered when the critical stress reaches σ_{crl}

‡ Tubes P1050-D203-1 and P1050-D203-2 did not experience ultimate failure due to test limitations

Table 3. Effect of Measured Ovalization on Moment of Inertia at Maximum Load

Specimen	d_{oval} (mm)	I_{oval} / I_o	P_{oval} / P_u
P350-D203-1	1.82	0.970	0.92
P350-D203-2	1.93	0.970	0.98
P700-D203-1	2.82	0.960	0.90
P700-D203-2	3.10	0.955	0.98
P700-D203-3	3.51	0.950	1.00
P1050-D203-1	2.30	0.965	1.00
P1050-D203-2	2.52	0.965	1.00
P1050-D203-3	1.71	0.970	0.93
Average	2.464	0.963	0.964
Standard Deviation	0.646	0.008	0.041

d_{oval} = ovalization; I_{oval} = moment of inertia of ovalized section; I_o = moment of inertia of original cross section; P_{oval} = load at last point that ovalization was measured; P_u = ultimate failure load of specimen

Table 4. Parametric Study Test Matrix

Inner Diameter	D/t	L/D
76.2	20	10,15*,20
	25	15
	30	15
	37	15
	45	10,15*,20
	50	15
	60	15
	70	15
	75	15
203.2	20	15
	25	15
	30	10,15*,20
	35	15
	43	10,15*,20
	52	15
	62	15
	68	15
	75	10,15*,20
304.8	23	15
	28	15
	34	15
	41	15
	47	15
	51	15
	57	15
	63	15
	72	15
406.4	22	15
	27	15
	33	15
	40	15
	48	15
	54	15
	62	15
	67	15
	74	15

** Matches a test specimen*

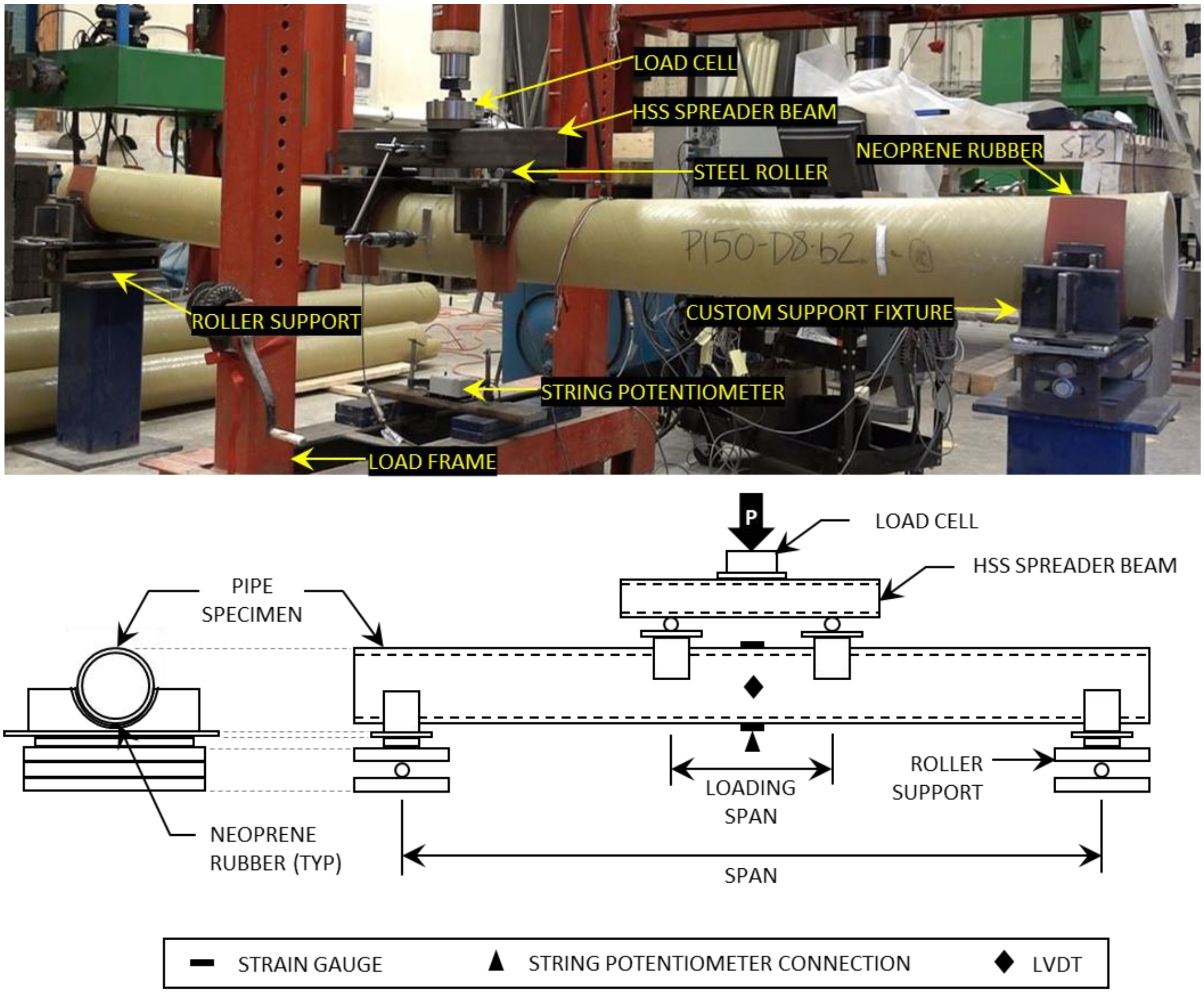

Figure 1. Test Set-up

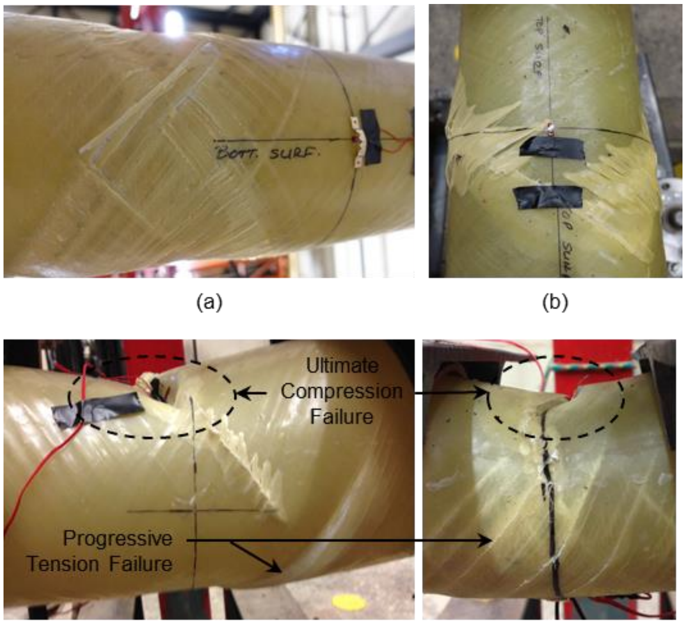

(a) (b)

(c) (d)

Figure 2. Photos of Typical Failure Mode: (a) Typical Bottom Face Progressive Tensile Failure; (b) Typical Top Face Ultimate Compression Failure (c) Side View of P350-D203 After Failure and; (d) Side View of P1050-D76 After Failure

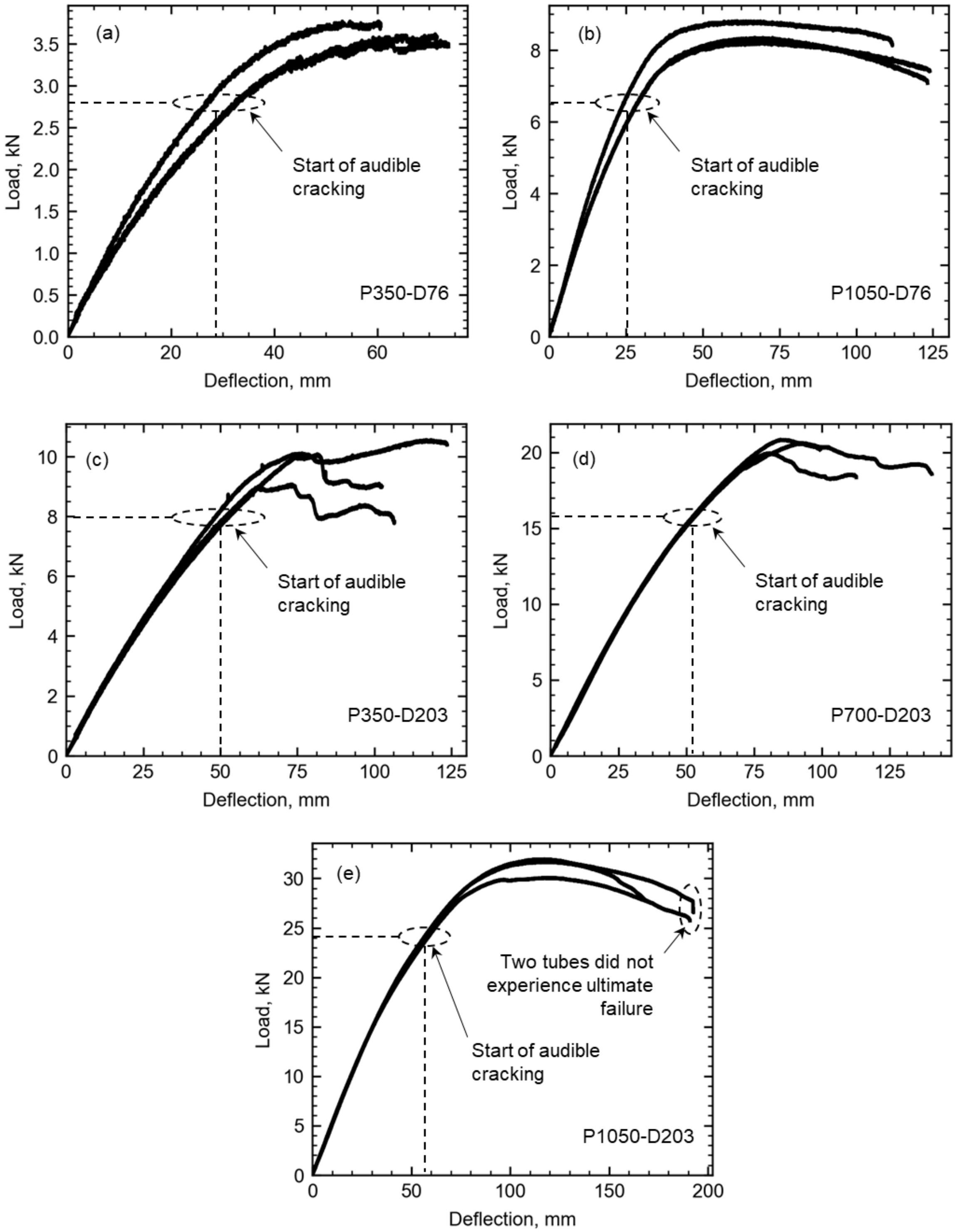

Figure 3. Load-Deflection Responses of (a) P350-D76; (b) P1050-D76; (c) P350-D203; (d) P700-D203 and; (e) P1050-D203

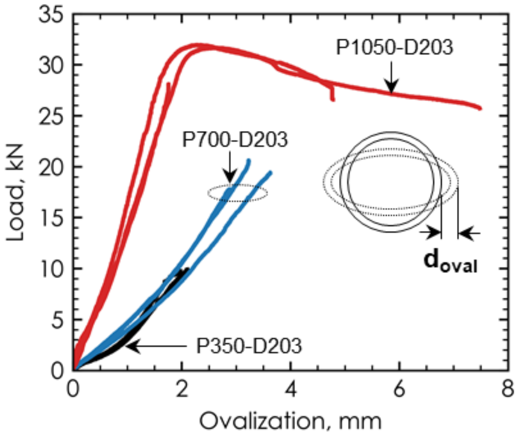

Figure 4. Measured Ovalization during Tube Bending Tests

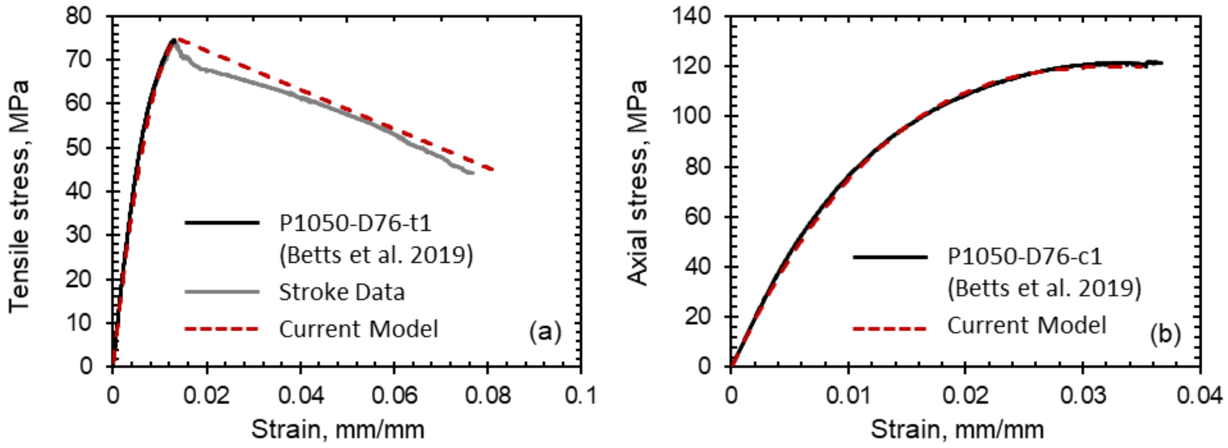

Figure 5. Model Verification of the Behavior of ±55° GFRP Tubes in (a) Tension and (b) Compression

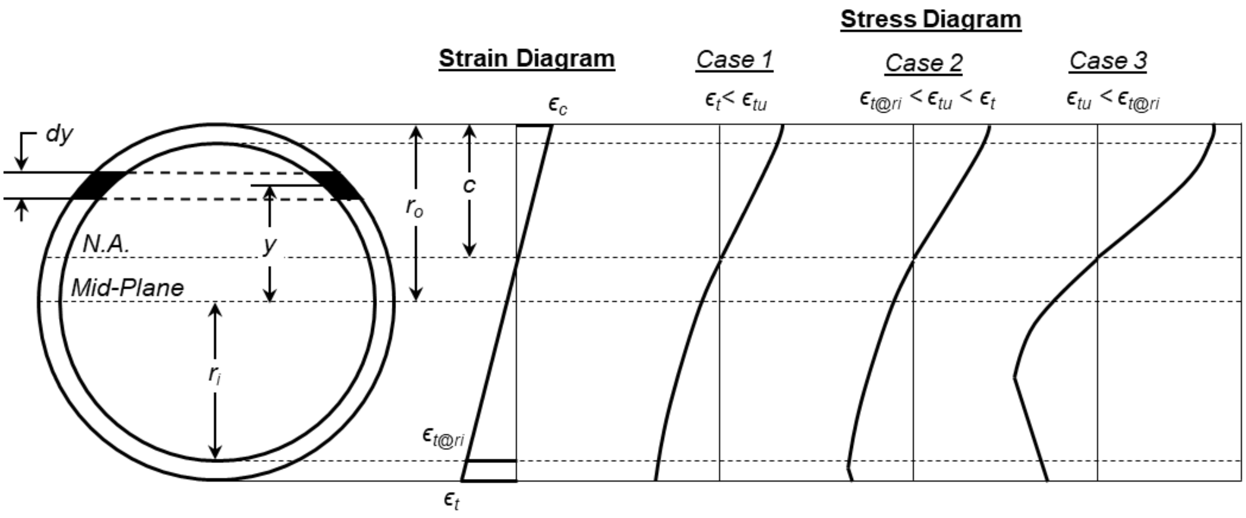

Figure 6. Cross Sectional Analysis of ±55° GFRP Tube

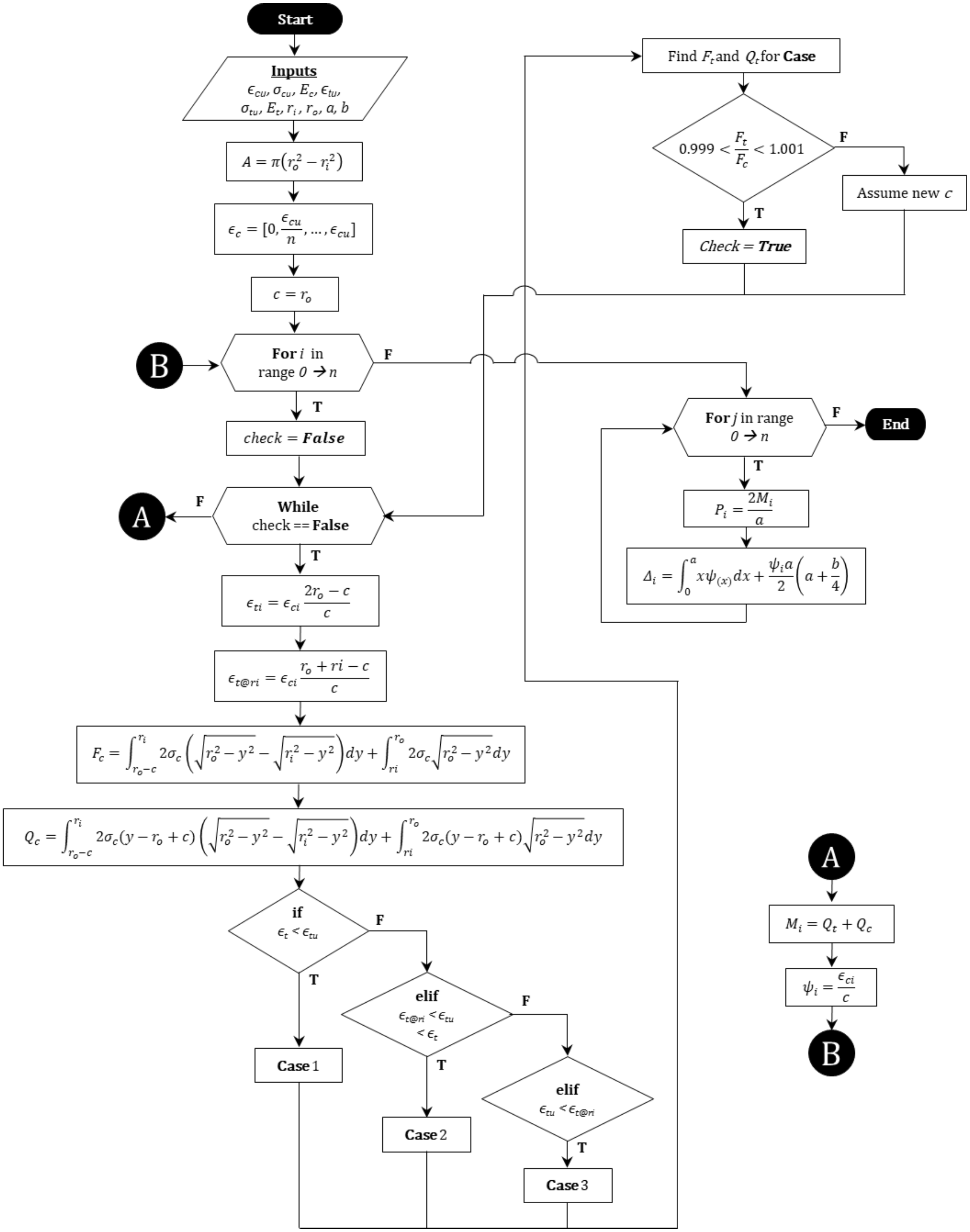

Figure 7. Analysis Procedure (Note that Case 1, Case 2 and Case 3 refer to the cases presented in Figure 6)

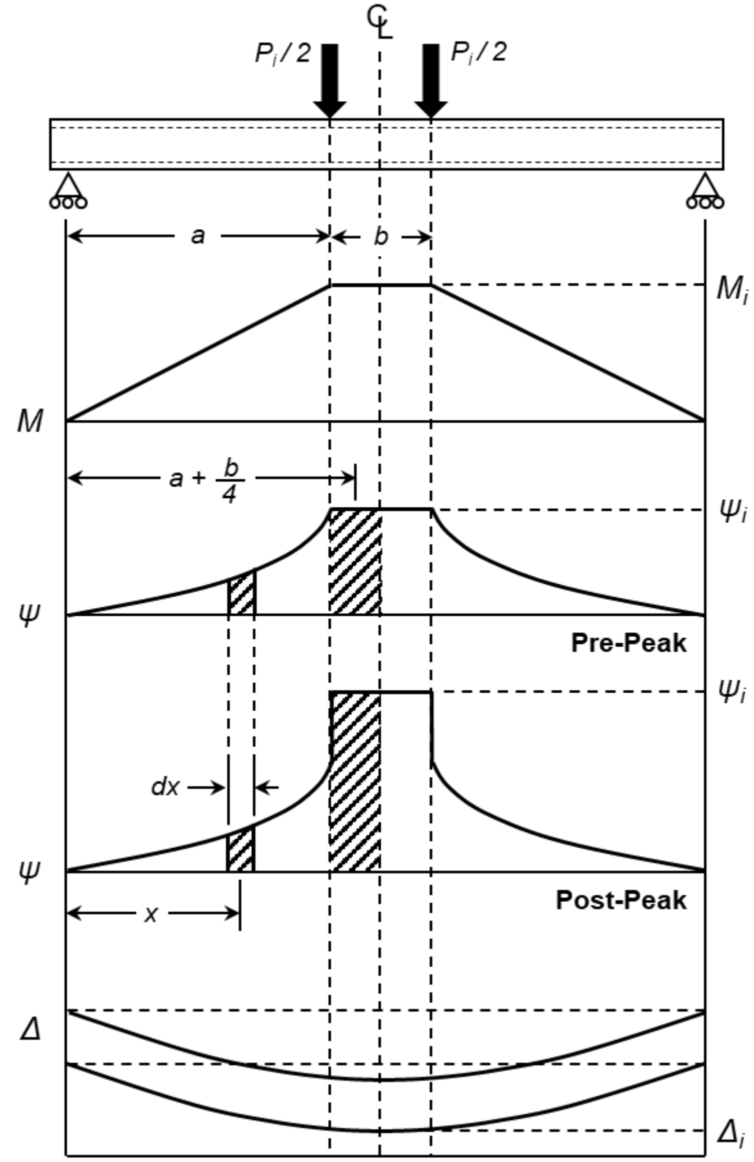

Figure 8. Determination of Tube Deflection

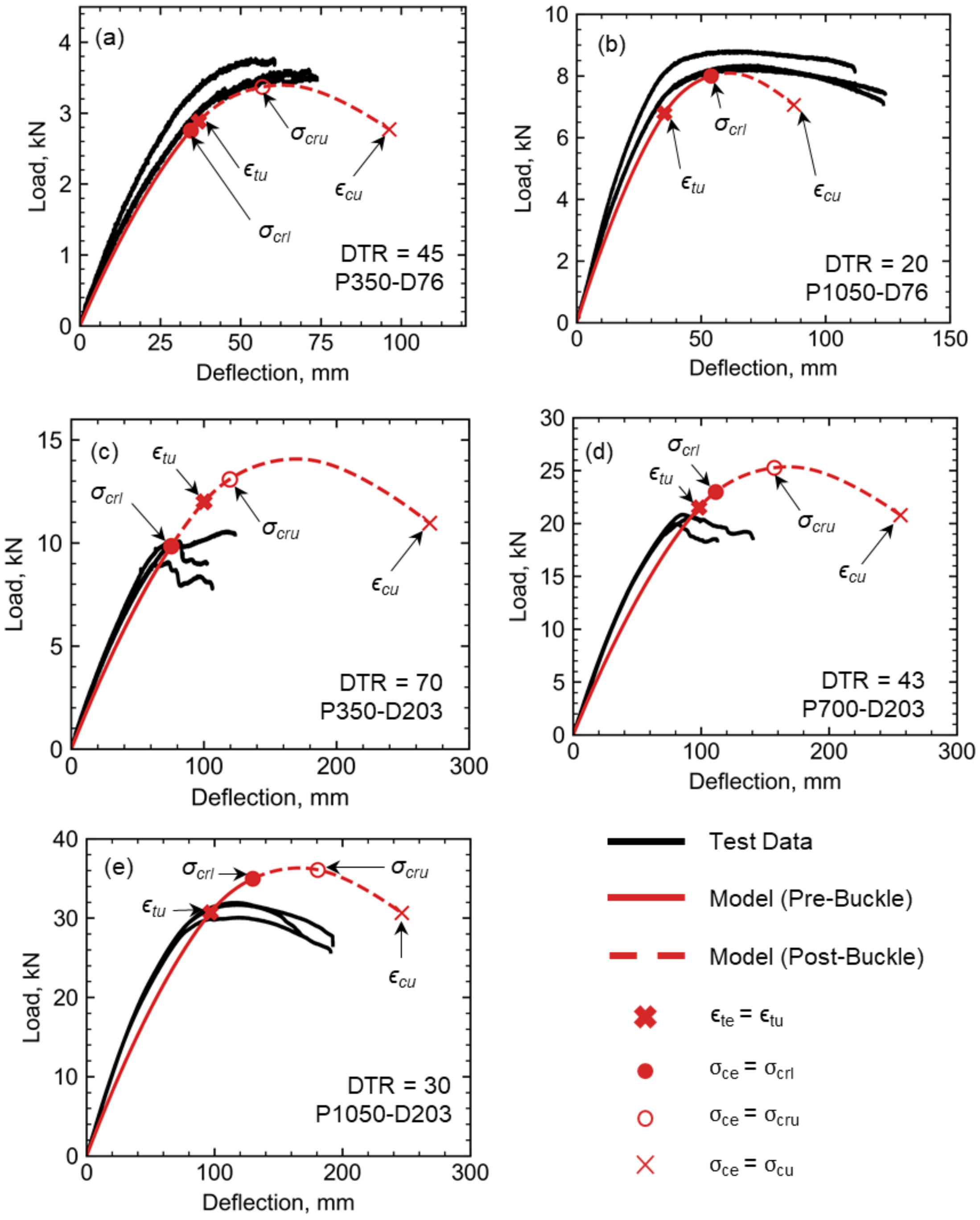

Figure 9. Model Verification: Load-Deflection of (a) P350-D76; (b) P1050-D76; (c) P350-D203; (d) P700-D203 and; (e) P1050-D203 (Note that the model is shown as a dashed line after σcrl)

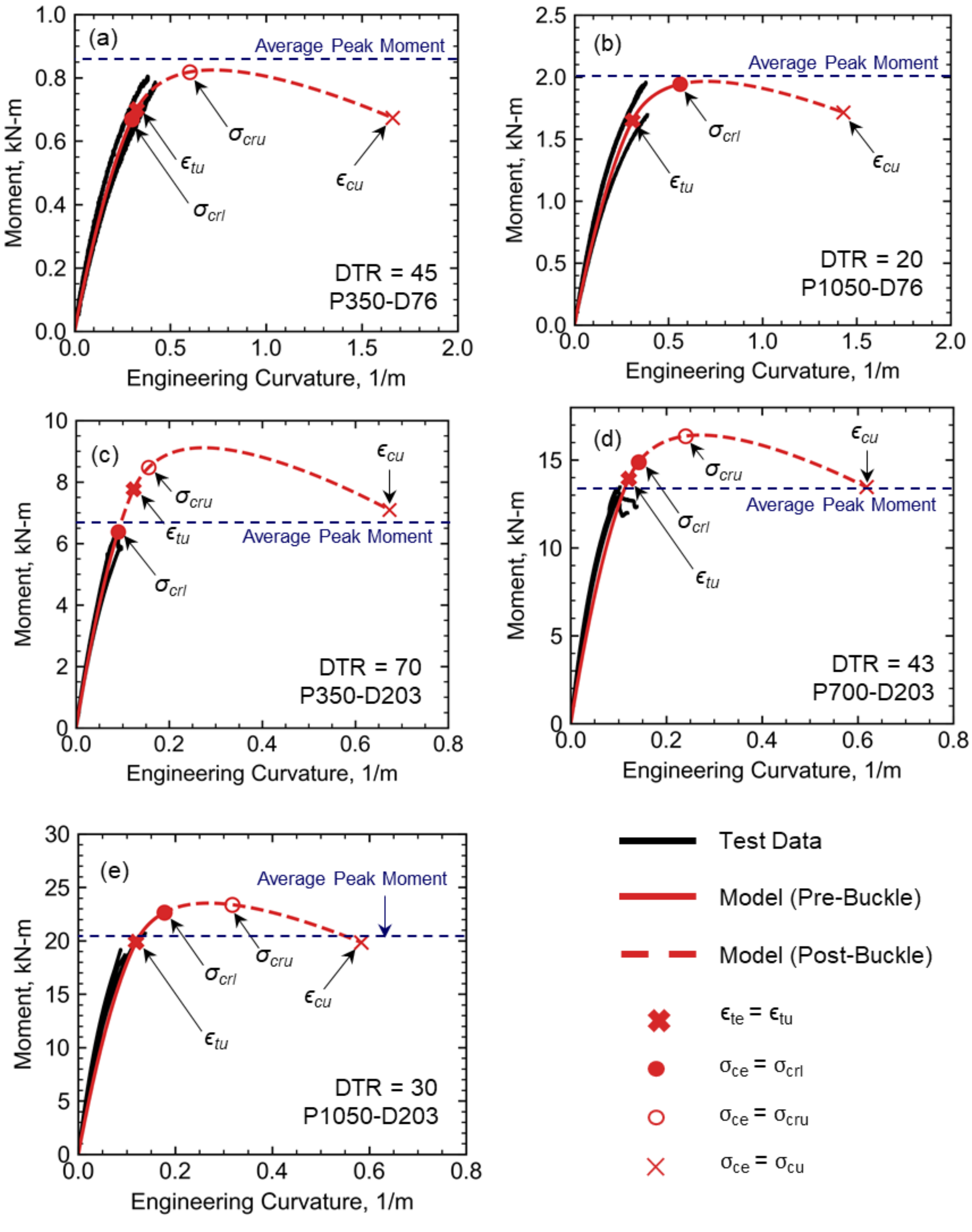

Figure 10. Model Verification: Moment-Curvature of (a) P350-D76; (b) P1050-D76; (c) P350-D203; (d) P700-D203 and; (e) P1050-D203 (Note that the strain gauge data used to calculate curvature was limited due to strain gauge failure during tests and that the model is shown as a dashed line after σ_{crl})

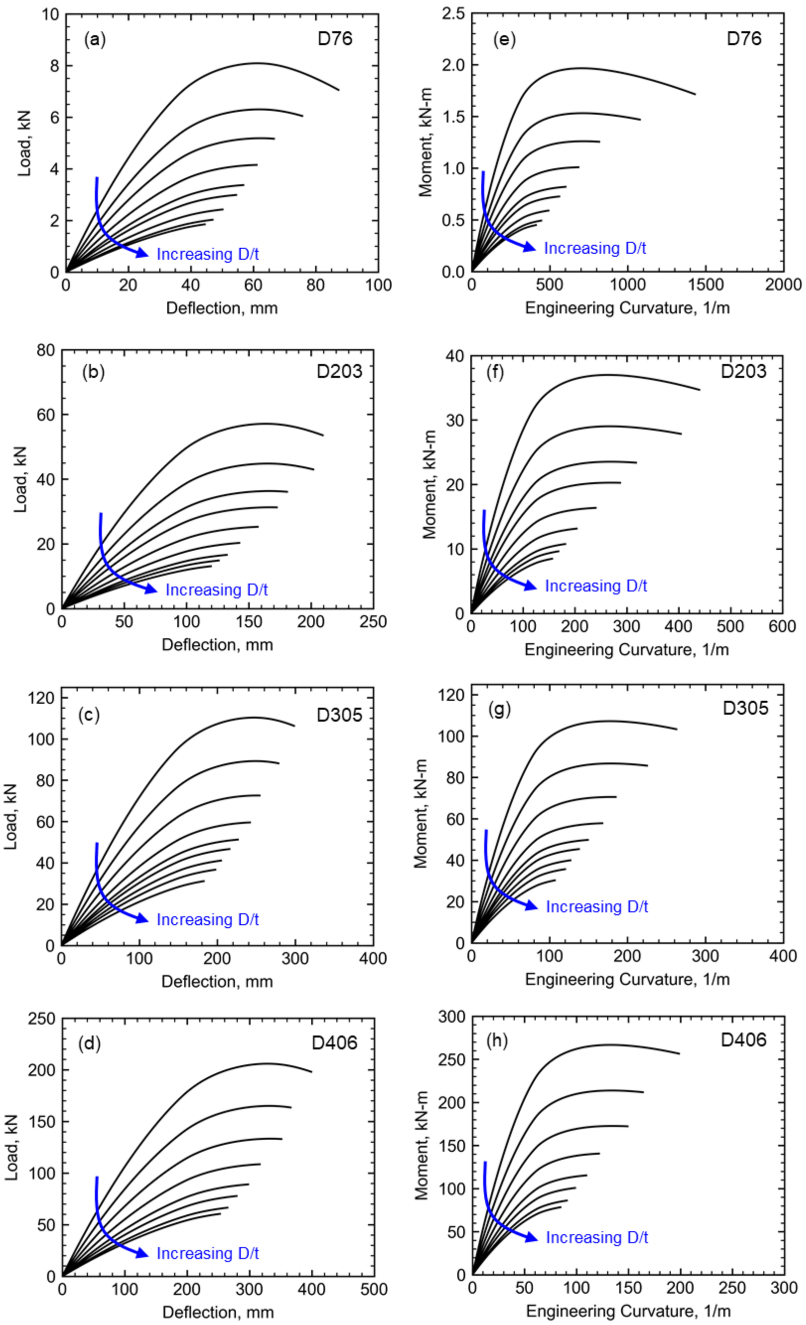

Figure 11. Effect of Diameter to Wall Thickness Ratio (D/t) on Load-Deflection of (a) D76; (b) D203; (c) D305; (d) D406 and Moment-Curvature of (e) D76; (f) D203; (g) D305; (h) D406

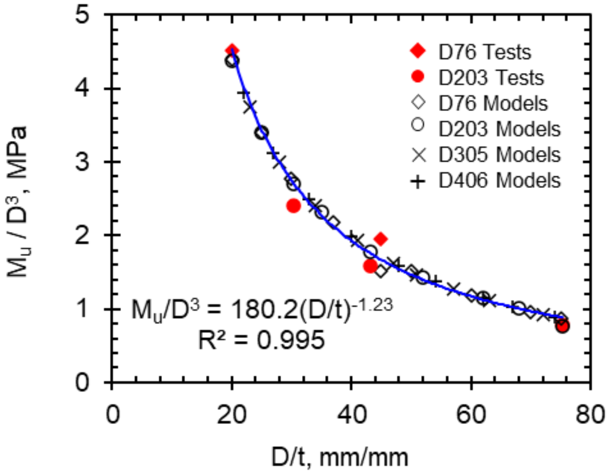

Figure 12. Effect of Diameter to Wall Thickness Ratio (D/t) on Moment Capacity of ±55° GFRP Tubes (Note that the test data for each specimen group is the average result of three tests)

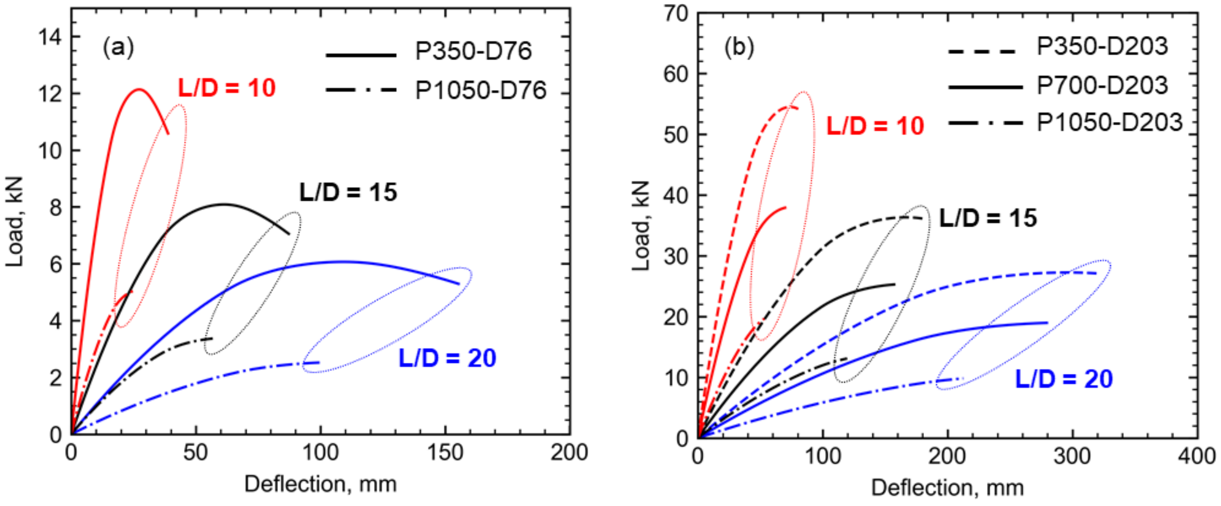

Figure 13. Effect of Span Length to Diameter Ratio (L/D) on Load-Deflection of (a) D76 and (b) D203